Applied Catalysis B: Environmental 259 (2019) 118020

Contents lists available at ScienceDirect

Applied Catalysis B: Environmental

journal homepage: www.elsevier.com/locate/apcatb

Rapid room-temperature fabrication of ultrathin $Ni(OH)_2$ nanoflakes with abundant edge sites for efficient urea oxidation

Wenlong Yang, Xianpeng Yang, Changmin Hou, Bijun Li, Hongtao Gao, Jiehua Lin, Xiliang Luo*

Key Laboratory of Optic-electric Sensing and Analytical Chemistry for Life Science, Ministry of Education, Shandong Key Laboratory of Biochemical Analysis, College of Chemistry and Molecular Engineering. Qingdao University of Science and Technology, Qingdao, 266042, China

ARTICLE INFO

Keywords:
Ultrathin nanosheets
Nickel hydroxide
Edge sites
Electrocatalysis
Urea oxidation

ABSTRACT

Ultrathin two-dimensional (2D) nanomaterials based on transition metal compounds can serve as alternative non-precious-metal electrocatalysts for urea oxidation reaction (UOR), which is vital to the development of direct urea fuel cells. Herein, we report a fast and room-temperature route to synthsize transition metal-based (Ni, Co, Mn) ultrathin 2D nanomaterials under ambient conditions. Theoretical and experimental studies demonstrate that the edges of $Ni(OH)_2$ are more active toward both the formation of NiOOH species and the adsorption of urea molecules than the basal planes, enabling accelerated catalytic kinetics for UOR. As expected, the β-$Ni(OH)_2$ nanoflakes manifest considerable electrocatalytic activity toward urea oxidation, reflecting 5.7 times higher current density (142.4 mA cm^{-2}) compared to the β-$Ni(OH)_2$ nanosheets at a potential of 0.6 V vs Ag/AgCl. This work brings great promise for the design of advanced electrode materials in the field of electrocatalysis.

1. Introduction

Urea electrolysis ($CO(NH_2)_2 + H_2O \rightarrow N_2 + 3H_2 + CO_2$) has been considered as an efficient route to produce hydrogen from urea-rich wastewater for the development of fuel cells, which helps to alleviate the growing energy crisis and environmental problems derived from the excessive depletion of fossil fuels [1–8]. However, the overall efficiency of this promising technique is severely limited by the intrinsically sluggish kinetics of urea oxidation reaction (UOR) due to its complex six-electron redox process ($CO(NH_2)_2 + 6OH^- \rightarrow N_2 + 5H_2O + CO_2 + 6e^-$) and gas evolution steps [9–11]. Therefore, appropriate UOR catalysts are usually required to expedite the kinetically sluggish process for realizing efficient urea electrolysis. Up to now, precious metal materials, such as platinum and rhodium have exhibit outstanding electrocatalytic activity towards UOR, while their scarce availability and high price seriously restrict the practical utilization on a large scale [12,13]. In this regard, tremendous efforts have been devoted to develop earth-abundant 3d transition metal compounds as alternative candidates for replacing the precious metal-based catalysts, because of their low cost, abundance of reserves and easy availability [14–20]. Nevertheless, the relatively poor electrocatalytic UOR performance of these transition metal-based catalysts needs to be further optimized to satisfy the requirement of practical application. Therefore, it is of significant importance to construct and synthesize low-cost, highly efficient and robust UOR catalysts aiming at the future commercialization of urea fuel cell.

In the past decade, two-dimensional (2D) nanosheets with ultrathin thickness have attracted considerable attention in the field of electrocatalysis, due to their great advantages such as large surface area, highly exposed active sites and modified electronic structures, which would bring great promise for the maximization of electrocatalytic performance [21–24]. To date, a series of effective methods including liquid exfoliation, size fractionation, *in situ* conversion, and hydrothermal treatment have been widely applied to synthesize ultrathin 2D nanosheets-based catalysts with small lateral sizes, yet these traditional routes generally involving prolonged process times or elevated pressures (or temperatures), are complicated, expensive and time-consuming [25–28]. Thus, developing a facile and time-efficient approach for fabricating ultrathin 2D nanosheets at room temperature and ambient atmosphere is highly desirable but remains a great challenge. It is noteworthy that, in most cases, the 3d transition metal-based catalysts should first undergo an oxidation reaction to form high-valence state metal sites before the oxidation of urea, whereas this electrochemical phase transformation process is unfortunately obstructed by the close-packed basal planes of 2D nanosheets [29–31]. Recent studies have proved that the atoms on the edges of 2D materials exhibit different properties and higher catalytic activity with respect to their basal planes [32–34]. Focused on this viewpoint, reducing the lateral size of

* Corresponding author.
E-mail address: xiliangluo@qust.edu.cn (X. Luo).

https://doi.org/10.1016/j.apcatb.2019.118020
Received 1 July 2019; Received in revised form 22 July 2019; Accepted 27 July 2019
Available online 30 July 2019

ultrathin 2D nanosheets is expected to be a general and feasible approach to expose more active edges for boosting the electrocatalytic activity. However, rare attention is paid to understanding the correlation between the active edges and UOR performance due to the lack of applicable catalyst model.

As a classic 3d transition metal-based material, nickel hydroxide ($Ni(OH)_2$) with intrinsic layered structure has been extensively studied and used as a promising UOR electrocatalyst due to its favorable activity and impressive stability in alkaline environment [10,34,35]. Herein, inspired by the above viewpoints, we put forward a fast and room-temperature synthetic strategy for transition metal-based catalysts with ultrathin 2D configuration at ambient atmosphere. Furthermore, taking the ultrathin $Ni(OH)_2$ nanosheets with small lateral sizes (denoted as Ni $(OH)_2$ nanoflakes) as an example, we get in-depth insights into the relationship between the active edges and UOR performance *via* a combination of theoretical calculations and experimental investigations, which reveals that the abundant active edges of $Ni(OH)_2$ nanoflakes can not only enable an accelerated phase transformation from Ni $(OH)_2$ to the electroactive NiOOH, but also favor the urea adsorption kinetics during the electrochemical process, thus giving greatly improved electrocatalytic activity for UOR. This work provides a comprehensive understanding of the positive effect of active edges on the electrocatalytic UOR performance, offering promising opportunities for future design and large-scale fabrication of high-efficiency UOR electrocatalysts.

2. Experimental section

2.1. Materials

All reagents were of analytical reagent grade, purchased from Sinopharm Chemical Reagent Co., Ltd., and used as received without further purification.

2.2. Synthesis of ultrathin $Ni(OH)_2$ nanoflakes

In a typical experiment, 1 mmol $NiCl_2{\cdot}6H_2O$ was dissolved in 200 mL water under vigorous magnetic stirring for 5 min followed by the adding of 1 mL of 28% ammonia solution to form a transparent solution. Then, 5 mL of ammonium persulfate aqueous solution (0.1 M) was added into the above solution drop by drop with vigorous stirring at room temperature. After several minutes, the precipitation was collected by centrifugation and then washed with distilled water and ethanol for three times, dried at 60 °C in air overnight for further characterization.

2.3. Preparation of ultrathin $Ni(OH)_2$ nanosheets

The ultrathin $Ni(OH)_2$ nanosheets were prepared according to a literature method [38]. Typically, 5 mmol $NiCl_2{\cdot}6H_2O$ was dissolved in 200 mL water with vigorous stirring for 5 min followed by the adding of 0.6 mL of 28% ammonia solution. Then, the obtained solution was transferred into a 500 mL three neck flask and heated at 60 °C for 24 h. After cooling to room temperature, the light green product was collected by centrifugation, washed by ethanol several times, and then dried at 60 °C in air overnight for further characterization.

2.4. Synthesis of other transition metal-based ultrathin nanosheets

The synthetic procedure for CoNi, CoMn and NiMn ultrathin nanosheets was similar to that for the ultrathin $Ni(OH)_2$ nanoflakes, except tuning the molar ratio of starting materials of $NiCl_2{\cdot}6H_2O$, $CoCl_2{\cdot}6H_2O$ and $MnCl_2{\cdot}4H_2O$ while keeping their total quantity at 1 mmol.

2.5. Characterization

Powder X-ray diffraction patterns (XRD) were obtain on Japan Rigaku D/max-rA equipped with graphite monochromatized high-intensity Cu Kα radiation ($\lambda = 1.54178$ Å). The transmission electron microscopy (TEM) images were conducted on a H-7650 (Hitachi, Japan) operated at an acceleration voltage of 100 kV. High-resolution transmission electron microscopy (HRTEM) and the corresponding electron diffraction (ED) analyses were carried out by using a JEOL-2010 TEM at an acceleration voltage of 200 kV. X-ray photoelectron spectroscopy (XPS) valence spectra were recorded on an ESCALAB MKII X-ray photoelectron spectrometer with an excitation source of Mg Kα $= 1253.6$ eV.

2.6. Electrochemical measurements

All of the electrochemical measurements were performed in a three-electrode system on an electrochemical station (CHI660B) at room temperature by using Ag/AgCl (3.3 M KCl) electrode as the reference electrode, a platinum wire as the counter electrode, and a glassy carbon electrode with different catalysts as the working electrode. In a typical procedure, 4 mg of catalysts and 30 μL of 5 wt % Nafion solutions (Sigma-Aldrich) were dispersed in 1 mL of water-isopropanol solution with volume ratio of 3:1 by sonicating for 1 h to form a homogeneous ink. After that, 5 μL of the above dispersion (containing 20 μg of catalyst) was load onto a glassy carbon electrode with a diameter of 3 mm (loading 0.285 mg cm^{-2}). Linear sweep voltammetry was carried out at a scan rate of 20 mV s^{-1} in 1 M KOH solution without and with 0.33 M urea. Electrochemical impedance spectroscopy (EIS) measurements of diffetent catalysts were carried out in 1 M KOH solution containing 0.33 M urea at 0.50 V vs Ag/AgCl. The amplitude of the applied voltage was 5 mV, and the frequency range was 100 K Hz to 1 Hz. Chronoamperometric measurement was performed in 1 M KOH solution containing 0.33 M urea at a constant potential of 0.45 V vs. Ag/AgCl.

3. Results and discussion

3.1. Catalyst characterization and discussion

In this study, the synthesis of $Ni(OH)_2$ nanoflakes with ultrathin thickness was accomplished by a simple liquid-phase reaction. As schematically illustrated in Fig. 1a, the precipitation was immediately generated with the addition of ammonium persulfate into an aqueous solution containing nickelammonia complex ($Ni[NH_3]_6^{2+}$) under ambient condition (experimental details in the Supporting Information). X-ray photoelectron spectra (XPS) in Figure S2 shows that only Ni and O elements can be detected in the obtained sample and the chemical state of Ni ions is divalent, verifying the presence of $Ni(OH)_2$ phase. Moreover, the structural information of as-obtained sample is disclosed by X-ray diffraction (XRD). As shown in Fig. 1b, all XRD diffraction peaks of the recollected powder can be readily indexed to hexagonal phase β-Ni $(OH)_2$, corresponding to JCPDS 73–1520 without any impurity phase, and the weak and broadened XRD peaks fairly reveal the small sizes of hexagonal β-$Ni(OH)_2$ crystalline. Transmission electron microscopy (TEM) was carried out to further survey the morphology of the product. As can be seen from the TEM images (Fig. 1c and Figure S1), the β-Ni $(OH)_2$ crystalline exhibits typical platelet-like morphology with uniform and small lateral size in the range of 20–40 nm, and the nearly transparent nature implies the ultrathin thickness of the synthesized β-$Ni(OH)_2$ nanoflakes. The high-resolution TEM (HRTEM) image (Fig. 1c, inset) displays the interplanar distances of 0.27 nm, matching well with that of (100) facet, indicative of the preferential exposure of the (001) basal plane of β-$Ni(OH)_2$ nanoflakes. Furthermore, the atomic force microscopic (AFM) image and corresponding height profiles in Fig. 1d and 1e reveal that the thickness of β-$Ni(OH)_2$ nanoflakes varies from 2.0 to 3.5 nm, approximately equaling to 4–7 β-$Ni(OH)_2$ layers along

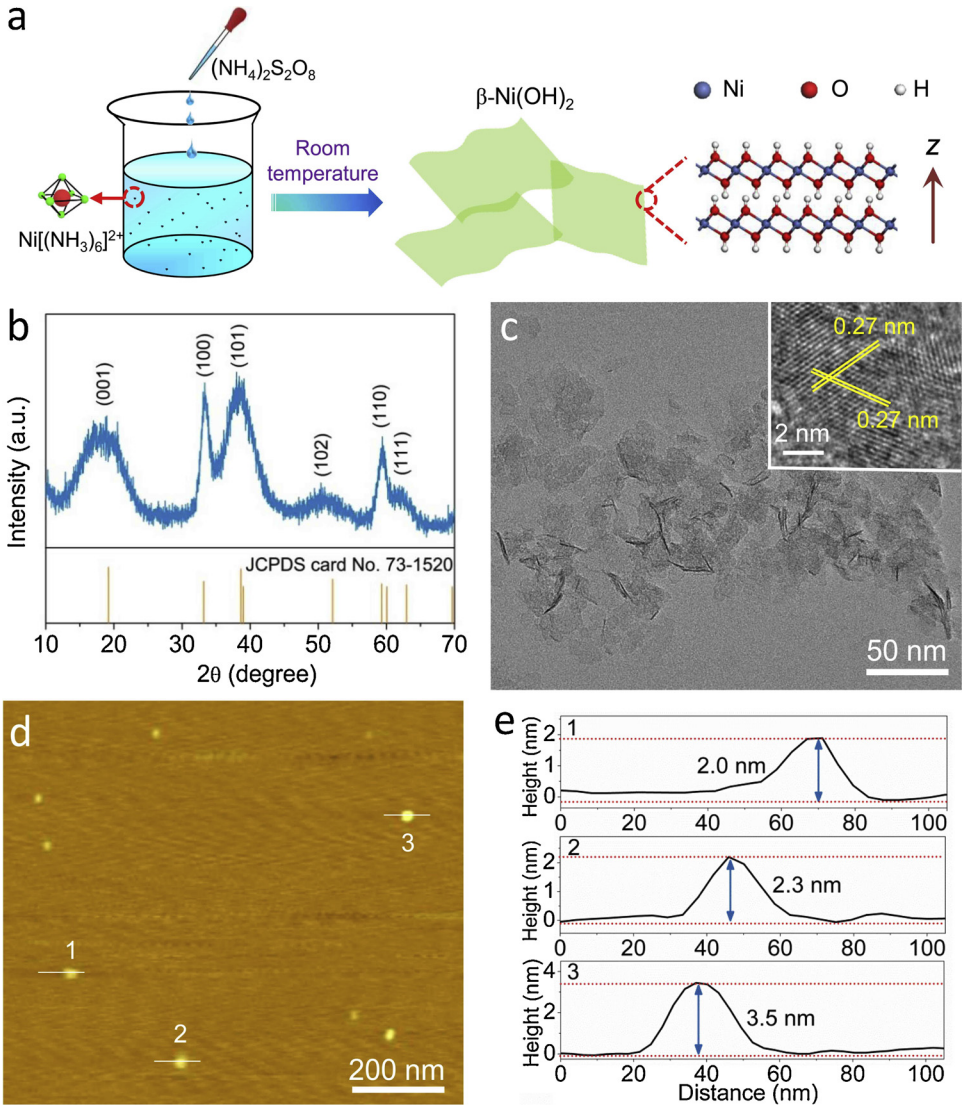

Fig. 1. (a) Schematic illustration for the synthesis of $Ni(OH)_2$ nanoflakes. (b) XRD pattern, (c) TEM and HRTEM images (inset), (d) AFM image and (e) corresponding height profiles of the as-obtained $Ni(OH)_2$ nanoflakes.

the [001] direction. On the basis of the above analyses, β-$Ni(OH)_2$ nanoflakes with ultrathin thickness have been successfully prepared at room temperature and ambient atmosphere through such a simple route. Interestingly, α-phase $Ni(OH)_2$ ultrathin nanosheets (Fig. 2a and Figure S3) can be also obtained when using an aqueous solution containing $NiCl_2$ and ammonium persulfate as the initiating agent followed by the addition of ammonium hydroxide. Of note, this method for fabricating ultrathin 2D nanosheets is not limited to $Ni(OH)_2$ but can be extended to a wide range of other 3d transition metal compounds, such as cobalt and manganese hydroxides or their corresponding double hydroxides. TEM images in Fig. 2 clearly illustrate that a variety of products with different components possess nanosheet morphology and ultrathin thickness, while XRD patterns in Figure S4 reveal their pure crystalline phase, unambiguously demonstrating the generality of this liquid-phase synthetic strategy. Meanwhile, the yield of ultrathin 2D nanosheets can be easily scaled up with only enlarging the size of reaction vessel, making it highly favorable for the large-scale production of nanosheets-based catalysts at low cost.

3.2. Evaluation of electrocatalytic activity for UOR

To shed light on the effect of active edges on the catalytic properties, ultrathin β-$Ni(OH)_2$ nanosheets with large lateral dimension were further synthesized as a reference catalyst. As shown in Figure S5, the lateral size ranging from 100 to 200 nm can be identified from the TEM image of obtained ultrathin β-$Ni(OH)_2$ nanosheets. Moreover, the Brunauer-Emmett-Teller (BET) plots in Figure S6 reveal that β-$Ni(OH)_2$ nanoflakes possess a very high specific surface area of 312.5 $m^2 g^{-1}$, roughly 4.2 times higher than that of β-$Ni(OH)_2$ nanosheets, which can be attributed to their ultrathin thickness and smaller lateral size. In order to evaluate the efficacy of active edges on the UOR performance, a series of electrochemical measurements were conducted by using glassy carbon (GC) electrode with catalyst loading of 0.285 mg cm^{-2} in a three-electrode system. The linear sweep voltammetry (LSV) curves of both $Ni(OH)_2$ nanoflakes and nanosheets catalysts were recorded in 1 M KOH solution with and without 0.33 M urea at a scan rate of 20 mV s^{-1}. As shown in Fig. 3a, an obvious oxidation peak at around 0.392 V vs. Ag/AgCl can be observed, corresponding to the phase transformation from β-$Ni(OH)_2$ to catalytically active β-NiOOH phase in KOH solution. Notably, the anodic current density of $Ni(OH)_2$ nanoflakes increases drastically as the potential becomes more positive after the addition of urea, indicating its fascinating electrocatalytic response capacity for UOR. By contrast, a mildly increased anodic current density after the addition of urea (Figure S7) demonstrates the mediocre catalytic

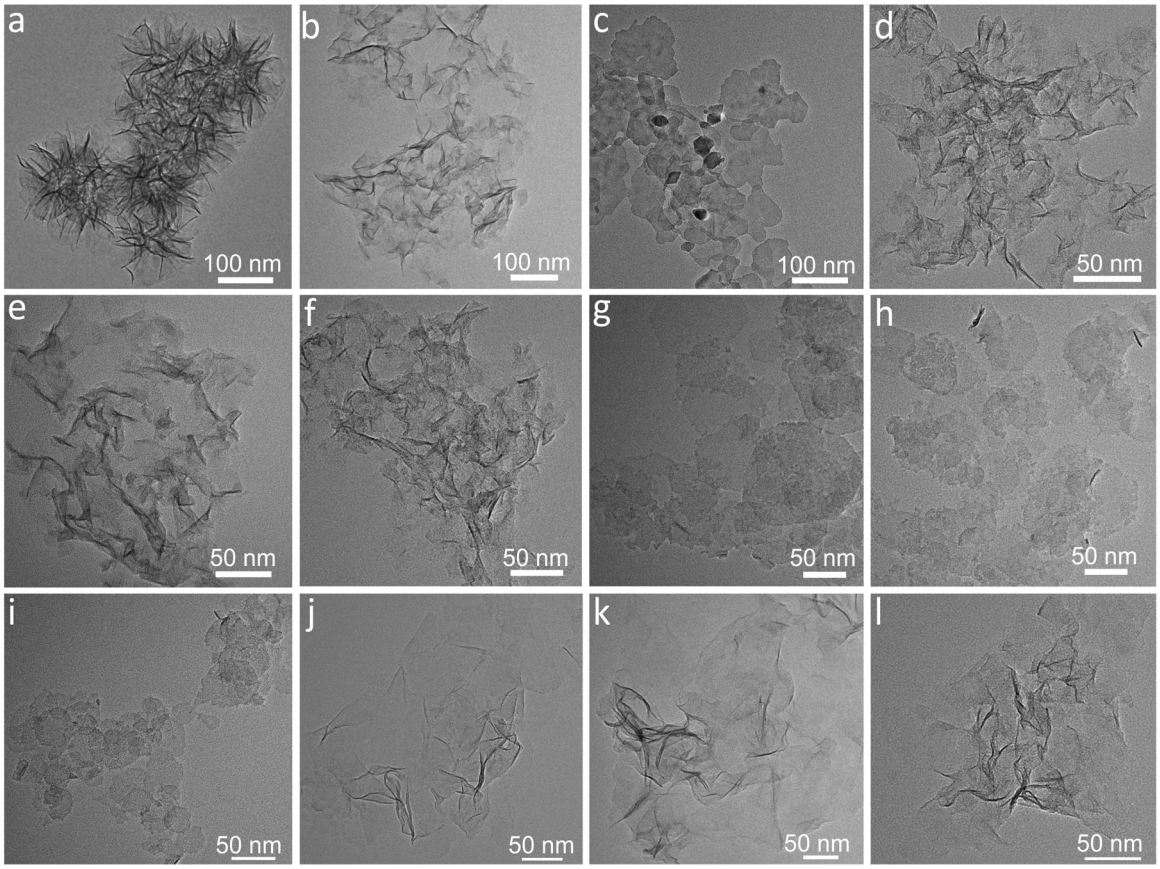

Fig. 2. TEM and HRTEM images of different ultrathin nanosheets: (a) α-$Ni(OH)_2$, (b) β-CoOOH, (c) β-MnOOH, (d) Co/Ni = 1/2, (e) Co/Ni = 1, (f) Co/Ni = 2, (g) Co/Mn = 1/2, (h) Co/Mn = 1, (i) Co/Mn = 2, (*j*) Ni/Mn = 1/2, (k) Ni/Mn = 1, (l) Ni/Mn = 2.

activity of $Ni(OH)_2$ nanosheets for UOR. Specifically, as can be seen from Fig. 3b, $Ni(OH)_2$ nanoflakes display a large anodic current density of 142.4 mA cm^{-2} at a potential of 0.6 V vs Ag/AgCl, which is 5.7 times larger than that of the $Ni(OH)_2$ nanosheets (24.8 mA cm^{-2}) and significantly higher than that of commercial 20% Pt/C [9]. Actually, to the best of our knowledge, this value is comparable to those of most reported high-activity catalysts measured on the GC electrode, or even on nickel foam or carbon cloth electrodes under similar conditions (Table S1). Moreover, the corresponding Tafel plots were employed to investigate the UOR kinetics of different catalysts. Fig. 3c shows that Ni $(OH)_2$ nanoflakes possess a Tafel slope of 36 $mVdec^{-1}$, much lower than that of $Ni(OH)_2$ nanosheets (153 $mVdec^{-1}$), revealing its favorable reaction kinetics of urea oxidation. Meanwhile, the electrochemical impedance spectroscopy (EIS) was further performed to survey the electrode kinetics for UOR. As shown in Fig. 3d, the Nyquist plots for Ni $(OH)_2$ nanoflakes exhibit a smaller semicircular diameter with respect to $Ni(OH)_2$ nanosheets, demonstrating that $Ni(OH)_2$ nanoflakes have a much smaller interfacial charge transfer resistance during the UOR process, which contributes to its superior UOR activity.

It is well accepted that active sites play the crucial role in determining the overall catalytic performance of catalysts. Therefore, the double-layer capacitance (C_{dl}), linearly proportional to the electrochemical active surface area (ECSA), was first conducted to evaluate the number of active sites. Cyclic voltammograms of different samples were measured from 1 mV s^{-1} to 10 mV s^{-1} at a non-faradaic potential region (Figure S8). As shown in Fig. 3e, the C_{dl} value of $Ni(OH)_2$ nanoflakes is calculated to be 768 μF cm^{-2}, which is roughly 1.46 times higher than that of $Ni(OH)_2$ nanosheets (525 μF cm^{-2}), confirming the larger ECSA of $Ni(OH)_2$ nanoflakes associated with its more exposed active edges. Besides the number of active sites, the intrinsic reactivity is another key factor in affecting the electrocatalytic performance. To further estimate the contribution of intrinsic reactivity of active sites to the enhanced UOR activity, the normalized LSV curves by ECSA were obtained in Fig. 3f. As can be seen, $Ni(OH)_2$ nanoflakes show a significantly larger normalized current densitiy, which is approximately 3.9-fold higher than that of $Ni(OH)_2$ nanosheets at a potential of 0.6 V vs Ag/AgCl, clearly revealing its superior intrinsic catalytic activity for UOR. According to these results, it is apparent that $Ni(OH)_2$ nanoflakes possess a much better UOR activity than $Ni(OH)_2$ nanosheets, unambiguously verifying the positive effect of the active edges on the urea oxidation.

3.3. Stability of electrocatalyst for UOR

Apart from UOR activity, electrochemical stability in alkaline media is another crucial criterion to evaluate an advanced electrocatalyst for practical applications. In this case, the chronoamperometry measurement for $Ni(OH)_2$ nanoflakes was carried out at a potential of 0.45 V vs Ag/AgCl in 1 M KOH solution containing 0.33 M urea. In Fig. 4a, only a slight decrease in anodic current density can be identified even after a long period of 30,000 s, demonstrating the excellent stability of Ni $(OH)_2$ nanoflakes for electrochemical urea oxidation in alkaline solution. Furthermore, TEM image in Fig. 4b gives evidence that $Ni(OH)_2$ nanoflakes still preserved the initial platelet-like morphology after the chronoamperometric response test, from which no obvious changes in the morphology can be observed, indicating its satisfactory structural durability in the electrocatalytic UOR process. Meanwhile, XPS analysis was conducted to survey the chemical state of nickel for the $Ni(OH)_2$ nanoflakes after UOR operation. As displayed in Fig. 4c, besides the peaks at 855.8 and 873.4 eV assigned to Ni^{2+}, the deconvoluted Ni 2p spectra exhibits two characteristic peaks at 857.2 and 873.4 eV, which can be respectively assigned to the $2p_{3/2}$ and $2p_{1/2}$ signals of Ni^{3+} [36],

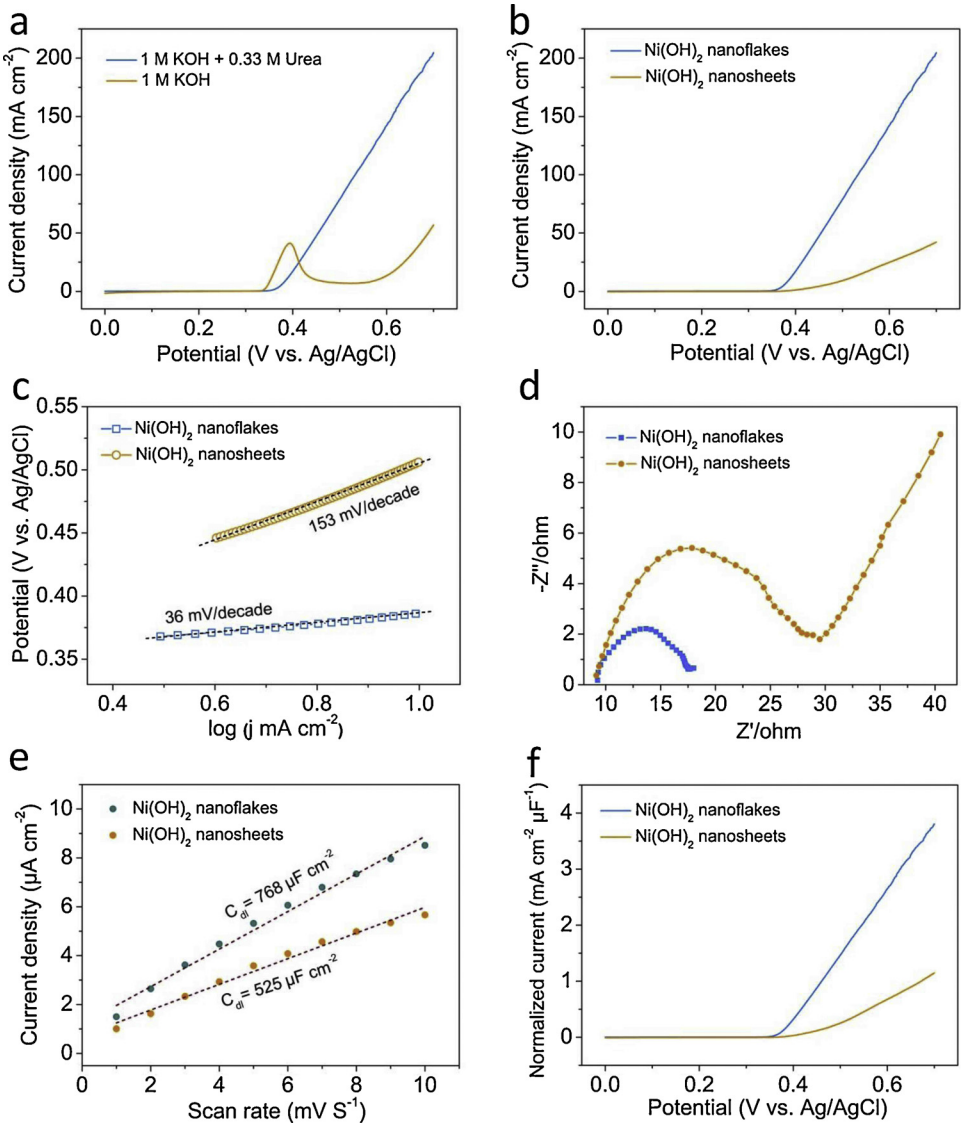

Fig. 3. (a) LSV curves of $Ni(OH)_2$ nanoflakes in 1 M KOH solution with and without 0.33 M urea at a scan rate of 20 mV s^{-1}. (b) LSV curves and (c) corresponding Tafel plots of $Ni(OH)_2$ nanoflakes and $Ni(OH)_2$ nanosheets in 1 M KOH solution containing 0.33 M urea. (d) Nyquist plots. (e) Estimation of the C_{dl} values. (f) LSV curves normalized by the C_{dl} values of $Ni(OH)_2$ nanoflakes and $Ni(OH)_2$ nanosheets.

confirming the existence of high oxidation states of Ni^{3+} cations as the catalytically active species for UOR. All of the above results illustrate that $Ni(OH)_2$ nanoflakes possess superior electrocatalytic activity as well as excellent stability toward urea oxidation, making it a promising anodic UOR catalyst for direct urea fuel cells.

3.4. Theoretical calculations for studying the effect of active edges on the increased electrocatalytic UOR performance

As mentioned above, the edges of nanosheet-based materials show significantly distinct local atomic arrangement in comparison to their basal planes, which reasonably results in different local electronic structures and physicochemical properties, giving the opportunity to optimize the poor UOR kinetics for improving the electrocatalytic UOR performance. In this case, density functional theory (DFT) calculations were performed to provide more insights into the contribution of active edges to the remarkable UOR activity. It is well-documented that the formation of active NiOOH from $Ni(OH)_2$ is the prerequisite for the electro-oxidation of urea, as high-valence Ni cations are regarded as the catalytically active species for UOR. As shown in Fig. 5b and Table S2, the formation energy of active β-NiOOH phase on the edges is calculated to be 1.76 eV, lower than that on the basal planes (2.14 eV), suggesting the easier formation of active species on the edges of β-$Ni(OH)_2$ catalyst. This viewpoint can be further confirmed by their cyclic voltammograms at different potential sweep rates as shown in Figure S9. The anodic peak current density (I_{pa}) of both catalysts increases gradually as the scan rate increases from 10 to 150 mV s^{-1}, which shows a nearly linear relation with the square root of scan rate ($v^{1/2}$). Obviously, Fig. 5a discloses that the slope value of linear plots (I_{pa} vs $v^{1/2}$) for $Ni(OH)_2$ nanoflakes (6.383) is much higher than that for $Ni(OH)_2$ nanosheets (2.736), revealing the better diffusion capacity of OH- on Ni $(OH)_2$ nanoflakes, which is more favorable for generating electroactive NiOOH species to facilitate the whole UOR process. Furthermore, the adsorption of urea molecules onto the surface of catalysts has been considered to be as another vital factor that can strongly affect the UOR performance since the catalyst-urea state is initially demanded for the onset of the urea oxidation [37]. As demonstrated by the DFT calculations in Fig. 5b and Table S3, the adsorption energy of urea onto the edge of β-$Ni(OH)_2$ is calculated to be -1.7056 eV, much smaller than that for the basal plane of β-$Ni(OH)_2$ (-0.3719 eV), indicating that the edges of β-$Ni(OH)_2$ are more active toward the adsorption of urea molecules with respect to the basal planes, which is conducive to

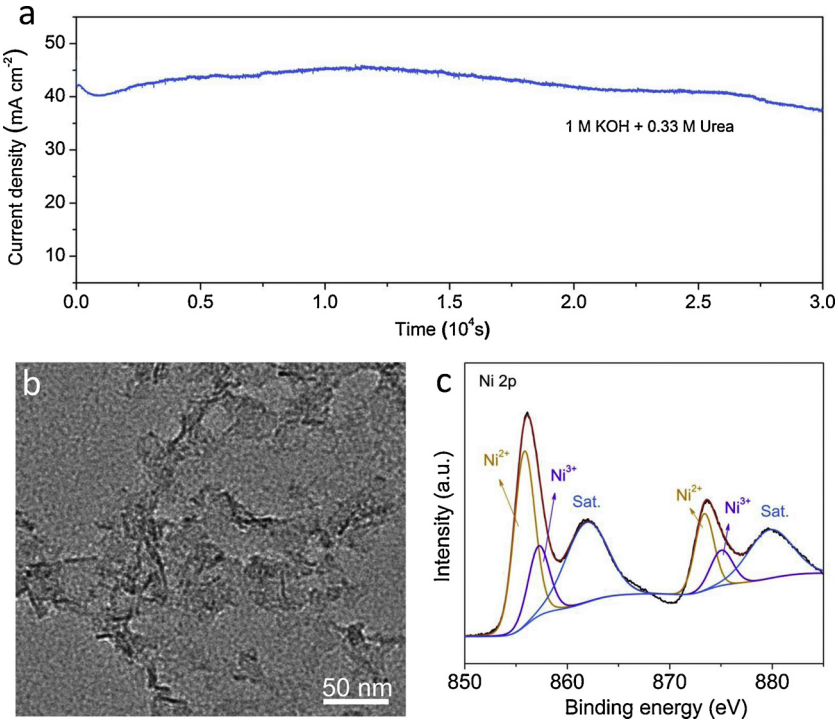

Fig. 4. (a) Chronoamperometric response of the $Ni(OH)_2$ nanoflakes electrode in 1 M KOH solution containing 0.33 M urea at the potential of 0.45 V vs Ag/AgCl. (b) TEM image and (c) XPS Ni 2p spectra of $Ni(OH)_2$ nanoflakes after the chronoamperometric test.

improving the slow reaction kinetics and thus the UOR performance. Moreover, the differential charge density in Fig. 5c and 5d illustrates that the Ni atoms on the edge of β-$Ni(OH)_2$ manifest a more prominent charge transfer with the adsorbed urea molecule in comparison with the Ni atoms on basal plane, implying the higher reactivity of active edges toward urea oxidation, which should be responsible for the superior eletrocatalytic UOR performance.

On the whole, $Ni(OH)_2$ nanoflakes show outstanding electrocatalytic UOR activity as well as excellent stability as a result of their unique ultrathin 2D structures and more exposed active edges. In detail, ultrathin 2D configuration enables the catalyst to possess a high contact area with the electrolyte and tight contact with the substrate electrode, which is beneficial for rapid interfacial electron transport and facile electrochemical reactions. Furthermore, the ultrathin thickness together with abundant active edges endow the $Ni(OH)_2$ nanoflakes with a large number of active sites, leading to greatly boosted surface reactions. Moreover, the more exposed active edges in the ultrathin Ni $(OH)_2$ nanoflakes not only decrease the energy required for the formation of active NiOOH phase from initial $Ni(OH)_2$, but also decrease the hindrance for the adsorption of urea molecules onto the surface of catalyst, both of which are in favor of a largely increased UOR rate.

4. Conclusions

In summary, a fast and universal method has been developed for the fabrication of transition metal-based 2D nanomaterials with ultrathin

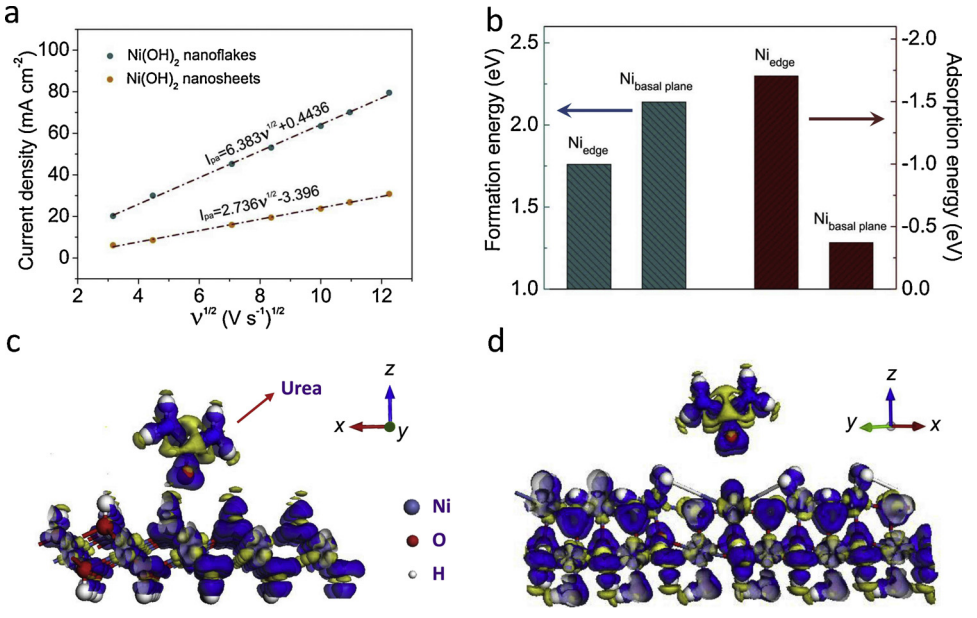

Fig. 5. (a) Linear relationship between the anodic peak current density and the square root of the scan rate ($I_{pa} \sim v^{1/2}$) for $Ni(OH)_2$ nanoflakes and $Ni(OH)_2$ nanosheets in 1 M KOH solution. (b) The calculated formation energies of β-NiOOH from β-$Ni(OH)_2$ and adsorption energies of urea molecule on the edge and basal plane of $Ni(OH)_2$ nanosheet. Illustration of the adsorption of urea molecule on the edge (c) and basal plane (d) of $Ni(OH)_2$ nanosheet and the corresponding differential charge density.

thickness and abundant active edges at room temperature. As a proof of concept prototype, the obtained ultrathin $Ni(OH)_2$ nanoflakes were further served as an advanced UOR electrocatalyst and ideal platform for revealing the underlying correlations between active edges and intrinsic catalytic properties during the UOR process. Benefiting from the increased electroactive surface area and reactivity of active sites, ultrathin $Ni(OH)_2$ nanoflakes exhibit superior electrocatalytic activity, with a larger current density and lower Tafel slope, and robust durability toward urea oxidation under alkaline conditions. Theoretical simulations demonstrated that the active edges of $Ni(OH)_2$ are more favorable for both the formation of electroactive NiOOH and the adsorption of urea molecules on the surface of catalyst, endowing the Ni $(OH)_2$ nanoflakes with optimal catalytic kinetics to accelerate the UOR process. This work not only presents an effective strategy to prepare ultrathin 2D nanosheets at room temperature, but also provides new perspectives for the future design of advanced non-precious-metal electrode materials to optimize the overall UOR performance, and thus promoting the commercialization of direct urea fuel cells.

Declaration of Competing Interest

The authors declare that they have no known competing financial interests or personal relationships that could have appeared to influence the work reported in this paper.

Acknowledgements

This work was supported by the National Natural Science Foundation of China (21675093, 41573103, 21422504, 21805149), the Natural Science Foundation of Shandong Province of China (ZR2018BB012, 2015ZRB01A0D), the Taishan Scholar Program of Shandong Province of China (ts20110829), and the Key Research and Development Program of Shandong Province of China (2017GSF16105, 2018GGX102004).

Appendix A. Supplementary data

Supplementary material related to this article can be found, in the online version, at doi:https://doi.org/10.1016/j.apcatb.2019.118020.

References

[1] G.M. Wang, Y.C. Ling, X.H. Lu, H.Y. Wang, F. Qian, Y.X. Tong, Y. Li, Solar driven hydrogen releasing from urea and human urine, Energy Environ. Sci. 5 (2012) 8215–8219.
[2] G.X. Wang, J.X. Chen, Y. Li, J.C. Jia, P.W. Cai, Z.H. Wen, Energy-efficient electrolytic hydrogen production assisted by coupling urea oxidation with a pH-gradient concentration cell, Chem. Commun. (Camb.) 54 (2018) 2603–2606.
[3] C. Lin, Z.F. Gao, F. Zhang, J.H. Yang, B. Liu, J. Jin, In situ growth of single-layered α-$Ni(OH)_2$ nanosheets on a carbon cloth for highly efficient electrocatalytic oxidation of urea, J. Mater. Chem. A Mater. Energy Sustain. 6 (2018) 13867–13873.
[4] F. Li, J.X. Chen, D.F. Zhang, W.F. Fu, Y. Chen, Z.H. Wen, X.J. Lv, Heteroporous MoS_2/Ni_3S_2 towards superior electrocatalytic overall urea splitting, Chem. Commun. (Camb.) 54 (2018) 5181–5184.
[5] Z.Y. Yu, C.C. Lang, M.R. Gao, Y. Chen, Q.Q. Fu, Y. Duan, S.H. Yu, Ni-Mo-O nanorod-derived composite catalysts for efficient alkaline water-to-hydrogen conversion via urea electrolysis, Energy Environ. Sci. 11 (2018) 1890–1897.
[6] Q. Liu, L.S. Xie, F.L. Qu, Z.A. Liu, G. Du, A.M. Asiri, X.P. Sun, A porous Ni_3N nanosheet array as a high-performance non-noble-metal catalyst for urea-assisted electrochemical hydrogen production, Inorg. Chem. Front. 4 (2017) 1120–1124.
[7] D.N. Liu, T.T. Liu, L.X. Zhang, F.L. Qu, G. Du, A.M. Asirie, X.P. Sun, High-performance urea electrolysis towards less energy-intensive electrochemical hydrogen production using a bifunctional catalyst electrode, J. Mater. Chem. A Mater. Energy Sustain. 5 (2017) 3208–3213.
[8] L.S. Xie, Q. Liu, Y. Luo, Z.A. Liu, Y.T. Xu, A.M. Asiri, X.P. Sun, F.Y. Xie, Bimetallic NiCoP nanosheets array for high-performance urea electro-oxidation and less energy-intensive electrolytic hydrogen production, ChemistrySelect 2 (2017) 10285–10289.
[9] D.D. Zhu, C.X. Guo, J.L. Liu, L. Wang, Y. Du, S.Z. Qiao, Two-dimensional metal-organic frameworks with high oxidation states for efficient electrocatalytic urea oxidation, Chem. Commun. (Camb.) 53 (2017) 10906–10909.
[10] X.J. Zhu, X.Y. Dou, J. Dai, X.D. An, Y.Q. Guo, L.D. Zhang, S. Tao, J.Y. Zhao, W.S. Chu, X.C. Zeng, C.Z. Wu, Y. Xie, Metallic nickel hydroxide nanosheets give superior electrocatalytic oxidation of urea for fuel cells, Angew. Chem. Int. Ed. 55 (2016) 12465–12469.
[11] J.F. Xie, H.C. Qu, F.C. Lei, X. Peng, W.W. Liu, L. Gao, P. Hao, G.W. Cui, B. Tang, Partially amorphous nickel-iron layered double hydroxide nanosheet arrays for robust bifunctional electrocatalysis, J. Mater. Chem. A Mater. Energy Sustain. 6 (2018) 16121–16129.
[12] B.K. Boggs, R.L. King, G.G. Botte, Urea electrolysis: direct hydrogen production from urine, Chem. Commun. (Camb.) 32 (2009) 4859–4861.
[13] A.T. Miller, B.L. Hassler, G.G. Botte, Rhodium electrodeposition on nickel electrodes used for urea electrolysis, J. Appl. Electrochem. 42 (2012) 925–934.
[14] M.R. Gao, W.C. Sheng, Z.B. Zhuang, Q.R. Fang, S. Gu, J. Jiang, Y.S. Yan, Efficient water oxidation using nanostructured α-Nickel-Hydroxide as an electrocatalyst, J. Am. Chem. Soc. 136 (2014) 7077–7084.
[15] J. Bao, X.D. Zhang, B. Fan, J.J. Zhang, M. Zhou, W.L. Yang, X. Hu, H. Wang, B.C. Pan, Y. Xie, Ultrathin spinel-structured nanosheets rich in oxygen deficiencies for enhanced electrocatalytic water oxidation, Angew. Chem. Int. Ed. 54 (2015) 7399–7404.
[16] Y.H. Liang, Q. Liu, A.M. Asiri, X.P. Sun, Enhanced electrooxidation of urea using $NiMoO_4{\cdot}xH_2O$ nanosheet arrays on Ni foam as anode, Electrochim. Acta 153 (2015) 456–460.
[17] K. Xu, P.Z. Chen, X.L. Li, Y. Tong, H. Ding, X.J. Wu, W.S. Chu, Z.M. Peng, C.Z. Wu, Y. Xie, Metallic nickel nitride nanosheets realizing enhanced electrochemical water oxidation, J. Am. Chem. Soc. 137 (2015) 4119–4125.
[18] G.X. Wang, Z.H. Wen, Self-supported bimetallic Ni-Co compound electrodes for urea- and neutralization energyassisted electrolytic hydrogen production, Nanoscale 10 (2018) 21087–21095.
[19] Y. Ding, Y. Li, Y.Y. Xue, B.Q. Miao, S.N. Li, Y.C. Jiang, X.E. Liu, Y. Chen, Atomically thick $Ni(OH)_2$ nanomeshes for urea electrooxidation, Nanoscale 11 (2019) 1058–1064.
[20] C. Tang, R. Zhang, W.B. Lu, Z. Wang, D.N. Liu, S. Hao, G. Du, A.M. Asiri, X.P. Sun, Energy-saving electrolytic hydrogen generation: Ni_2P nanoarray as a high-performance non-noble-Metal electrocatalyst, Angew. Chem. Int. Ed. 56 (2017) 842–846.
[21] W.L. Yang, X.D. Zhang, Y. Xie, Advances and challenges in chemistry of two-dimensional nanosheets, Nano Today 11 (2016) 793–816.
[22] Y.F. Sun, S. Gao, F.C. Lei, C. Xiao, Y. Xie, Ultrathin two-dimensional inorganic materials: new opportunities for solid state nanochemistry, Acc. Chem. Res. 48 (2015) 3–12.
[23] H. Zhang, Ultrathin two-dimensional nanomaterials, ACS Nano 9 (2015) 9451–9469.
[24] D.H. Deng, K.S. Novoselov, Q. Fu, N.F. Zheng, Z.Q. Tian, X.H. Bao, Catalysis with two-dimensional materials and their heterostructures, Nature Nanotech. 11 (2016) 218–230.
[25] F. Song, X.L. Hu, Ultrathin cobalt-manganese layered double hydroxide is an efficient oxygen evolution catalyst, J. Am. Chem. Soc. 136 (2014) 16481–16484.
[26] S. Chen, J.J. Duan, A. Vasileff, S.Z. Qiao, Size fractionation of two-dimensional sub-nanometer thin manganese dioxide crystals towards superior urea electrocatalytic conversion, Angew. Chem. Int. Ed. 55 (2016) 3804–3808.
[27] S.Q. Wang, Z.Q. Zhu, P.W. Li, C.H. Zhao, C.J. Zhao, H. Xia, In situ conversion of sub-4 nm $Co(OH)_2$ nanosheet arrays from phytic acid-derived $Co_3(HPO_4)_2(OH)_2$ for superior high loading supercapacitors, J. Mater. Chem. A Mater. Energy Sustain. 6 (2018) 20015–20024.
[28] X.M. Zhou, Z.M. Xia, Z.Y. Zhang, Y.Y. Ma, Y.Q. Qu, One-step synthesis of multi-walled carbon nanotubes/ultra-thin Ni(OH)2 nanoplate composite as efficient catalysts for water oxidation, J. Mater. Chem. A Mater. Energy Sustain. 2 (2014) 11799–11806.
[29] L. Trotochaud, J.K. Ranney, K.N. Williams, S.W. Boettcher, Solution-cast metal oxide thin film electrocatalysts for oxygen evolution, J. Am. Chem. Soc. 134 (2012) 17253–17261.
[30] M.S. Burke, M.G. Kast, L. Trotochaud, A.M. Smith, S.W. Boettcher, Cobalt-iron (Oxy)hydroxide oxygen evolution electrocatalysts: the role of structure and composition on activity, stability, and mechanism, J. Am. Chem. Soc. 137 (2015) 3638–3648.
[31] J.F. Xie, J.P. Xin, R.X. Wang, X.D. Zhang, F.C. Lei, H.C. Qu, P. Hao, G.W. Cui, B. Tang, Y. Xie, Sub-3 nm pores in two-dimensional nanomesh promoting the generation of electroactive phase for robust water oxidation, Nano Energy 53 (2018) 74–82.
[32] X.R. Wang, Y.J. Ouyang, L.Y. Jiao, H.L. Wang, L.M. Xie, J. Wu, J. Guo, H.J. Dai, Graphene nanoribbons with smooth edges behave as quantum wires, Nat. Nanotechnol. 6 (2011) 563–567.
[33] B. Ni, X. Wang, Edge overgrowth of spiral bimetallic hydroxides ultrathin-nanosheets for water oxidation, Chem. Sci. 6 (2015) 3572–3576.
[34] J. Hu, B.L. Huang, C.X. Zhang, Z.L. Wang, Y.M. An, D. Zhou, H. Lin, M.K.H. Leung, S.H. Yang, Engineering stepped edge surface structures of MoS_2 sheet stacks to accelerate the hydrogen evolution reaction, Energy Environ. Sci. 10 (2017) 593–603.
[35] J.F. Xie, X.D. Zhang, H. Zhang, J.J. Zhang, S. Li, R.X. Wang, B.C. Pan, Y. Xie, Intralayered ostwald ripening to ultrathin nanomesh catalyst with robust oxygen-evolving performance, Adv. Mater. 29 (2017) 1604765.
[36] Q. He, Y.Y. Wan, H.L. Jiang, Z.W. Pan, C.Q. Wu, M. Wang, X.J. Wu, B.J. Ye, P.M. Ajayan, L. Song, Nickel vacancies boost reconstruction in nickel hydroxide electrocatalyst, ACS Energy Lett. 3 (2018) 1373–1380.
[37] Y. Tong, P.Z. Chen, M.X. Zhang, T.P. Zhou, L.D. Zhang, W.S. Chu, C.Z. Wu, Y. Xie, Oxygen vacancies confined in nickel molybdenum oxide porous nanosheets for promoted electrocatalytic urea oxidation, ACS Catal. 8 (2018) 1–7.
[38] H. Zhou, J.B. Peng, X.L. Qiu, Y.S. Gao, L.M. Lu, W.M. Wang, β-$Ni(OH)_2$ nanosheets: an effective sensing platform for constructing nucleic acid-based optical sensors, J. Mater. Chem. B Mater. Biol. Med. 5 (2017) 7426–7432.